Quantum interference in exciton-Mn spin interactions in a CdTe semiconductor quantum dot

Trojnar, A. H.; Korkusinski, M.; Kadantsev, E. S.; Hawrylak, P.; Goryca, M.

Publisher's version / Version de l'éditeur:
http://dx.doi.org/10.1103/PhysRevLett.107.207403
Physical Review Letters, 107, 20, pp. 207403-1-207403-5, 2011-11-11

Quantum Interference in Exciton-Mn Spin Interactions in a CdTe Semiconductor Quantum Dot

A. H. Trojnar,[1,2] M. Korkusiński,[1] E. S. Kadantsev,[1] P. Hawrylak,[1,2] M. Goryca,[3] T. Kazimierczuk,[4] P. Kossacki,[3,4] P. Wojnar,[5] and M. Potemski[3]

[1]*Institute for Microstructural Sciences, National Research Council, Ottawa, Canada*
[2]*Department of Physics, University of Ottawa, Ottawa, Canada*
[3]*Grenoble High Magnetic Field Laboratory, CNRS, Grenoble, France*
[4]*Institute of Experimental Physics, University of Warsaw, Warsaw, Poland*
[5]*Institute of Physics, Polish Academy of Sciences, Warsaw, Poland*

(Received 31 March 2011; published 11 November 2011)

We show theoretically and experimentally the existence of a new quantum-interference effect between the electron-hole interactions and the scattering by a single Mn impurity. The theoretical model, including electron–valence-hole correlations, the short- and long-range exchange interaction of a Mn ion with the heavy hole and with electron and anisotropy of the quantum dot, is compared with photoluminescence spectroscopy of CdTe dots with single magnetic ions. We show how the design of the electronic levels of a quantum dot enables the design of an exciton, control of the quantum interference, and hence engineering of light-Mn interaction.

DOI: 10.1103/PhysRevLett.107.207403 PACS numbers: 78.67.Hc, 71.70.Gm, 78.55.Et

Isolating and controlling states of a single quantum spin, an atomic limit of quantum memory, either on a surface of a metal [1,2] or in a semiconductor quantum dot (QD) [3–10], is at an early stage. In semiconductor quantum dots [6–10], a manganese (Mn) ion with magnetic moment $M = 5/2$ has been detected by observation of a characteristic excitonic emission spectrum consisting of six emission lines related to the $2M + 1 = 6$ possible Mn quantum states [6–9]. The emission spectrum has been interpreted using a spin model where the exciton spin interacts with the spin of the Mn ion, while all electron-hole correlations were neglected [6–14]. However, only a microscopic treatment presented here of an exciton as a correlated excited state of the interacting quantum dot and the Mn as an impurity allows for full control of exciton-Mn coupling. This problem is related to the nontrivial enhancement of the electron-electron interactions by impurities [15] as well as the Kondo effect [16].

Here we show theoretically and experimentally how one can manipulate the spin of Mn ion with light in a semiconductor quantum dot by engineering Mn-exciton interactions through design of a quantum-dot exciton [17,18]. A new quantum-interference (QI) effect between the electron-hole Coulomb scattering and the scattering by Mn ion is shown to significantly reduce the exciton-Mn coupling revealed by a characteristic pattern in the emission spectrum. Engineering light-Mn spin interaction opens up new applications in quantum memory and information processing.

In the effective mass approximation, an exciton [17,18] is composed of an electron with spin $\sigma = 1/2$ and a valence heavy hole with spin $\tau = 3/2$, each occupying single-particle states $|i\rangle = |n, m\rangle$ of a two-dimensional harmonic oscillator with quantum numbers n and m and energy $\varepsilon_i = \omega(n + m + 1)$ [19,20], shown in Fig. 1(a), where ω is the shell energy spacing. The energy is measured in effective Rydbergs ($\mathcal{R}^* = m^* e^4/2\varepsilon^2\hbar^2$), length in effective Bohr radius ($a_B = \varepsilon/m_e^* e^2$), where m_e^* is an electron effective mass, e an electron charge, and ε is the dielectric constant. For CdTe $m_e^* = 0.1$, $\varepsilon = 10.6$, $\mathcal{R}^* = 12.11$ meV, and $a_B = 5.61$ nm.

The state of an electron-hole pair $|i, j\rangle|\sigma, \tau\rangle$ is a product of the orbital part and the spin part. The lowest energy state, labeled $|a\rangle$ in Fig. 1(a), corresponds to the electron and the hole on the s shell ($n = 0$, $m = 0$) while excited states $|b\rangle$ and $|c\rangle$ correspond to both the electron and the hole excited from the s shell to the p shell ($n = 1$, $m = 0$; $n = 0$, $m = 1$). If the d shell is present in the quantum dot, another pair of excited states [labeled $|g\rangle$ and $|h\rangle$ in Fig. 1(a)] at a similar energy is possible where either the hole or the electron is excited from the s shell to the zero angular momentum state ($n = 1$, $m = 1$) of the d shell. The s, p, and d shells of a single, nonmagnetic CdTe quantum dot studied here appear as emission maxima with an increasing excitation power, as shown in Fig. 1(b). By rotating the electron-hole configurations to Jacobi coordinates [18], one finds that there are only three low-energy electron-hole configurations: $|A\rangle = |a\rangle$, $|B\rangle = (1/\sqrt{2})(|b\rangle + |c\rangle)$, and $|H\rangle = (1/\sqrt{2})(|h\rangle + |g\rangle)$ coupled by Coulomb interactions. Higher energy states $|D\rangle, |E\rangle, |F\rangle$, involving both an electron and a hole on a d shell, have twice the energy of configurations $|B\rangle$, $|C\rangle$, $|G\rangle$, and $|H\rangle$, contribute little to the exciton ground state, are not essential for the effect discussed here, and are neglected in the qualitative discussion but included in all numerical calculations. We will also refer to the $|A\rangle$, $|B\rangle$, and $|H\rangle$ configurations as $|SS\rangle$, $|PP\rangle$, and $|SD\rangle$, respectively. Only configurations $|SS\rangle$ and $|PP\rangle$ are optically active, but

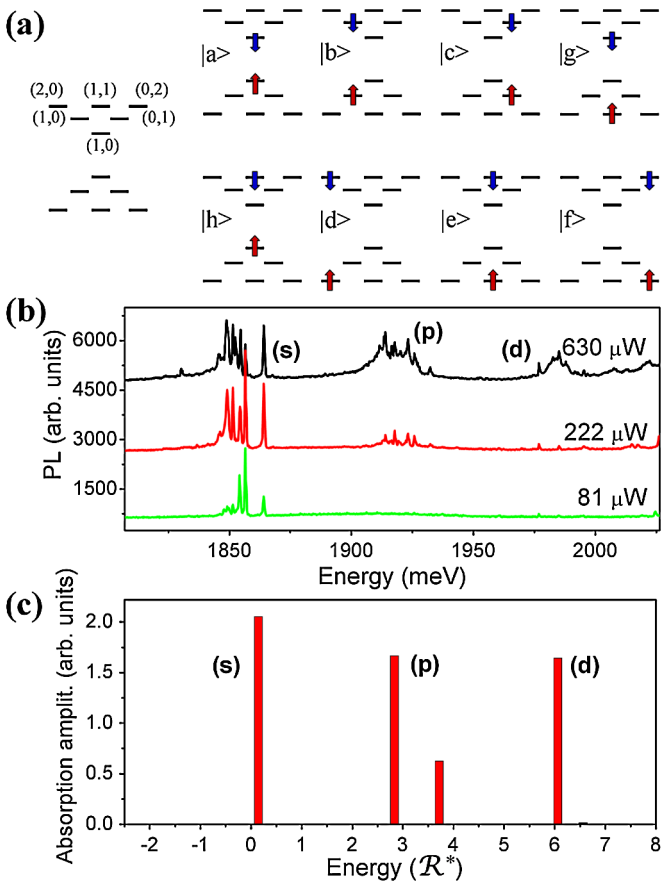

FIG. 1 (color online). (a) The electron and hole shell structure $\varepsilon_{n,m}$ and basic two-particle configurations. Electron (hole) is marked by the down-pointing blue (up-pointing red) arrows. (b) Measured emission spectra from s, p, and d shells of a reference, nonmagnetic single CdTe quantum dot populated with increasing number of electron-hole pairs with increasing excitation power (details of growth follow in the text). (c) Calculated absorption spectrum of a CdTe isotropic quantum dot without electron-hole exchange, with the single-particle energies $\omega_e + \omega_h = 30$ meV, $\omega_e = \omega_h$, and energy measured from band gap energy of CdTe.

Coulomb scattering couples all three exciton configurations, and, in particular, the degenerate configurations $|PP\rangle$ and $|SD\rangle$ [18]. By diagonalizing the electron-hole Hamiltonian $H_{e\text{-}h} = \sum_{i\tau}\varepsilon^h_{i\tau}h^\dagger_{i\tau}h_{i\tau} + \sum_{i\sigma}\varepsilon^e_{i\sigma}c^\dagger_{i\sigma}c_{i\sigma} - \sum_{ijkl\sigma\tau}\langle i, j|V_{e\text{-}h}|k, l\rangle c^\dagger_{i\sigma}h^\dagger_{j\tau}h_{k\tau}c_{l\sigma}$ [where $h^\dagger_{i\tau}$ ($c^\dagger_{i\sigma}$) and $h_{i\tau}$ ($c_{i\sigma}$) create and annihilate hole (electron) on the orbital i with spin $\tau(\sigma)$] in the space of all configurations, we obtain the ground and excited states as well as the absorption spectrum, shown in Fig. 1(c).

We see that for a quantum dot with s-d shells the p-shell exciton spectrum splits into two lines due to the $|SD\rangle$ configuration resonant with the $|PP\rangle$ configuration [18], and, correspondingly, contributes to the ground state $|\mathrm{GS}\rangle$ of the exciton. The ground state can be approximated as $|\mathrm{GS}\rangle = A_{ss}|SS\rangle + A_{pp}|PP\rangle - A_{sd}|SD\rangle$. We note that the $|PP\rangle$ and $|SD\rangle$ configurations contribute to the $|\mathrm{GS}\rangle$ with opposite signs, a result of different signs of Coulomb matrix elements $\langle SS|V|PP\rangle = -\langle SS|V|SD\rangle$, connecting the $|PP\rangle$ and $|SD\rangle$ configurations with the $|SS\rangle$ configuration.

The interacting electron-hole-Mn system is described by the Hamiltonian [12]: $H_X = H_{e\text{-}h} + H_{\mathrm{EHX}} + H_{\mathrm{anis}} + H_{\mathrm{Zeeman}} + H_{h\text{-Mn}} + H_{e\text{-Mn}}$. The first term is the electron-hole Hamiltonian $H_{e\text{-}h}$, the second term is the electron-hole exchange term [21] $H_{\mathrm{EHX}} = \sum_{ijkl\sigma\sigma'\tau\tau'}\langle i\sigma, j\tau|V^X_{e\text{-}h}|k\tau', l\sigma'\rangle c^\dagger_{i\sigma}h^\dagger_{j\tau}h_{k\tau'}c_{l\sigma'}$, the third is the anisotropic potential term $H_{\mathrm{anis}} = \sum_{ij\tau}t^h_{ij}h^\dagger_{i\tau}h_{j\tau} + \sum_{ij\sigma}t^e_{ij}c^\dagger_{i\sigma}c_{i\sigma}$ which breaks the cylindrical symmetry of the quantum dot and mixes the single-particle states with different angular momenta. The anisotropy is characterized by ω_x and ω_y [22], giving the cylindrically symmetrical component of the parabolic confinement as $\omega^2_{0,e(h)} = \frac{1}{2}(\omega^2_{x,e(h)} + \omega^2_{y,e(h)})$, while the anisotropic component $t^{e(h)}_{ij}$ is proportional to the anisotropy parameter $\gamma_{e(h)} = (\omega^2_{x,e(h)} - \omega^2_{y,e(h)})/2\omega^2_{0,e(h)}$. The fourth term is the Zeeman energy of the magnetic ion, the spin of the hole and of the electron $H_{\mathrm{Zeeman}} = g_{\mathrm{Mn}}\mu_B BM_Z + g_e\mu_B BS_Z + g_h\mu_B BJ_Z$, where g_e (g_h) are electron (hole) Lande g factors and μ_B the Bohr magneton. The hole-Mn ion Hamiltonian $H_{h\text{-Mn}} = \sum_{i,j}\frac{3J^h_{ij}(R)}{2}[(h^\dagger_{i,\Uparrow}h_{j,\Uparrow} - h^\dagger_{i,\Downarrow}h_{j,\Downarrow})M_Z]$ describes the scattering of the hole by the Mn ion while conserving the hole spin. $J^h_{ij}(R) = J^h_{2\mathrm{D}}\Psi^*_i(R)\Psi_j(R)$ is the effective exchange matrix element leading to the scattering of a hole from state i to state j by the Mn ion at position R [12,23]. This scattering process does depend on the spin state of the Mn ion. The electron-Mn interaction term is similar to the hole-Mn scattering term except for the additional spin flipping term $H_{e\text{-Mn}} = -\sum_{i,j}\frac{J^e_{ij}(R)}{2}[(c^\dagger_{i,\uparrow}c_{j,\uparrow} - c^\dagger_{i,\downarrow}c_{j,\downarrow})M_Z + c^\dagger_{i,\downarrow}c_{j,\uparrow}M^+ + c^\dagger_{i,\uparrow}c_{j,\downarrow}M^-]$. The electron-Mn interaction strength is $J^e_{2\mathrm{D}} = 2J^e_{(0)}/d$, where $J^e_{(0)} = 15$ meV $\cdot$ nm^3 (Refs. [12,23]) and $d = 2.56$ nm is the height of the QD. The h-Mn coupling $J^h_{(0)} = 60$ meV $\cdot$ nm^3 is 4 times larger. The exciton-Mn configurations are a product of exciton states discussed in Fig. 1(a), electron-hole spin configurations, and states of Mn ion, e.g., $|\mathrm{GS}\rangle|\Uparrow\downarrow\rangle|M_Z\rangle$.

We now turn to evaluating the exchange interaction of the exciton with the Mn spin. Its dominant component is the valence hole-Mn Ising-like interaction, and for qualitative description we focus on it here [12,24]. The spin of the hole plays the role of the effective magnetic field, leading to the "exchange" splitting of different M_Z states: $\langle H_{h\text{-Mn}}\rangle = \langle M_Z|\langle\downarrow\Uparrow|\langle \mathrm{GS}|H_{h\text{-Mn}}|\mathrm{GS}\rangle|\Uparrow\downarrow\rangle|M_Z\rangle = \alpha M_Z$.

With p orbitals not coupled to the Mn in the center of the dot [23] and $|\mathrm{GS}\rangle = A_{ss}|SS\rangle + A_{pp}|PP\rangle - A_{sd}|SD\rangle$, we find:

$$\langle H_{h\text{-Mn}}\rangle = \frac{3}{2}[A^{*2}_{ss}J_{ss} - \sqrt{2}A_{ss}A_{ds}J_{sd}]M_Z. \qquad (1)$$

We see that the exchange splitting $\alpha = 3/2[A_{ss}^{*2}J_{ss} - \sqrt{2}A_{ss}A_{ds}J_{sd}]$ of Mn levels is a difference of two terms. The first term $A_{ss}^{*2}J_{ss}$ is proportional to the product of the sum of probability amplitudes of the hole occupying s and d orbitals $A_{ss}^{*2} = A_{ss}^2 + A_{ds}^2$ in the exciton GS weighted by the exchange matrix element $J_{dd} = J_{ss}$. The second term, $-\sqrt{2}A_{ss}A_{ds}J_{sd}$, reduces the magnitude of the exchange. This term is proportional to the product $A_{ds}J_{sd}$, i.e., the amplitude A_{ds} of the $|SD\rangle$ configuration in the exciton GS, present only due to the electron-hole Coulomb interaction and scattering matrix element J_{sd} of the hole by the Mn ion acting as an impurity. Hence both the electron-hole Coulomb interactions and the scattering by the Mn impurity must be simultaneously present to reduce the hole exchange field. This is the QI effect, the central result of this work. The QI is absent in shallow quantum dots with s-p shells but takes place in quantum dots with at least three confined shells. The same conclusion holds for Mn off center but with A_{ss}^* renormalized by the J_{pp} coupling.

We now turn to the second signature of QI: coupling of the ground and excited exciton states by Mn-ion spin acting as a scattering center. The first excited exciton orbital state $|ES\rangle = B_{sd}|SD\rangle + B_{pp}|PP\rangle + B_{ss}|SS\rangle + \cdots$ is a linear combination of configurations $|SD\rangle$ and $|PP\rangle$ with a small admixture of the $|SS\rangle$ configuration. The coupling of exciton-Mn states with exciton in its ground $|\mathrm{GS}\rangle|\sigma\tau\rangle|M_Z\rangle$ and excited orbital state $|\mathrm{ES}\rangle|\sigma\tau\rangle|M_Z\rangle$ by the hole-Mn exchange interaction $\langle M_Z|\langle\downarrow\Uparrow|\langle \mathrm{GS}|H_{h\text{-}\mathrm{Mn}}|\mathrm{ES}\rangle|\Uparrow\downarrow\rangle|M_Z\rangle = \kappa M_Z$ turns out to be proportional to the state of the Mn spin M_Z. The excited state renormalizes the energies of the ground state exciton-Mn spin complex $E_{\mathrm{GS}}^{M_Z} = E_{\mathrm{GS}} + \alpha M_Z - (\frac{\kappa^2 M_Z^2}{\Delta E - (\beta-\alpha)M_Z})$, where β is the exchange splitting of the Mn levels in the excited exciton state $|\mathrm{ES}\rangle$ with energy E_{ES} and $\Delta E = E_{\mathrm{ES}} - E_{\mathrm{GS}}$. The main result is the nonuniform and renormalized spacing of Mn energy levels in the exciton-Mn s-shell complex:

$$\Delta_{M_Z} = E_{\mathrm{GS}}^{M_Z+1} - E_{\mathrm{GS}}^{M_Z} = \left(\alpha - \frac{\kappa^2}{\Delta E}\right) - \frac{2\kappa^2 M_Z}{\Delta E}. \quad (2)$$

Figure 2(a) shows the results of numerical calculations of the average spacing of Mn energy levels in the s shell as a function of the number of shells, including electron-hole direct Coulomb interaction and electron-Mn and hole-Mn interactions for parameters typical for a CdTe quantum dot. Indeed, we see that the spacing is reduced by a factor of 2 when the quantum dot admits the d shell. The renormalization of s-shell Mn energy levels by the excited exciton state is shown schematically in Fig. 2(b). We see that the ground and excited levels corresponding to the same M_Z are coupled by Mn, the coupling strength is different for each M_Z leading to energy shift, with states with higher $|M_Z|$ shifting more, which in turn leads to a nonuniform spacing of levels. The differences in the magnitude of this shift are visualized in Fig. 2(b) in the form of different lengths of arrows, with the solid (dashed) vertical lines representing the exciton-Mn energy levels with (without) the ground state-excited state coupling.

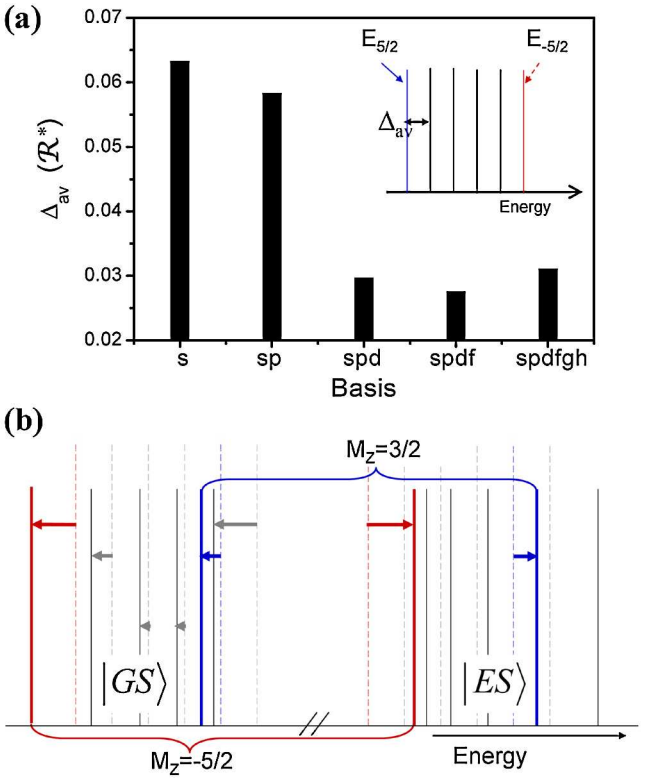

FIG. 2 (color online). (a) Calculated average spacing [$\Delta_{\mathrm{av}} = (E_{-5/2} - E_{5/2})/5$] of Mn energy levels in the s shell as a function of the number of shells of an isotropic CdTe quantum dot with negligible electron-hole exchange, with single-particle energies $\omega_e + \omega_h = 30$ meV; $\omega_e/\omega_h = 4$. (b) Schematic renormalization of ground $|\mathrm{GS}\rangle$ and excited $|\mathrm{ES}\rangle$ exciton-Mn complex energy levels by the interaction with excited states of an exciton. Levels corresponding to the same Mn-ion spin projection repel each other, with the strength proportional to M_Z. Dashed (solid) vertical lines represent the energy levels of the X-Mn system in the s-shell (six lines on the left) and the p-shell (six lines on the right) energy region unrenormalized (renormalized) by the interaction, whose magnitude is represented by the horizontal arrows.

The experimental spectra of the emission from quantum dots were obtained for CdTe-based heterostructures, which were grown using molecular beam epitaxy. Each of them contains a single layer of self-assembled CdTe QDs with a low concentration of Mn^{2+} ions, embedded in a ZnTe matrix. The density of quantum dots was about 5×10^9 cm^{-2}. The Mn^{2+} concentration was adjusted to obtain a significant number of QDs containing exactly one Mn^{2+} ion [25]. For the measurements, the sample was placed in a microphotoluminescence setup composed of piezoelectric x-y-z stages and a microscope objective. The system was kept at the temperature of 4.2 K in a helium

exchange gas. The photoluminescence (PL) of the QDs was excited either above the gap of the ZnTe barrier (at 532 nm) or using a tunable dye laser in the range 570–610 nm. Both the exciting and the collected light were transmitted through a monomode fiber coupled directly to the microscope objective. The overall spatial resolution of the setup was better then 1 μm which assured the possibility of selecting different single quantum dots containing a single Mn^{2+} ion. The dots without Mn^{2+} ion were observed in the same samples. The PL analysis was done for the dots having emission lines in the low-energy tail of the broad PL emission band [9,25], which assured good separation from the lines related to the other dots. The characteristic PL spectra contain a neutral exciton line split into sextuplets. Lower in energy, the lines related to charged excitons (X^+ and X^-) and biexciton were observed. Higher in energy, the emission from higher shells ($s, p, d, \ldots$) appear with an increasing excitation power, as is shown in Fig. 1(b). From many quantum dots those with emission spectra with six emission lines, i.e., Mn in the center of a dot [26], were selected.

Figure 3(a) shows the measured and numerically calculated emission spectrum from the s shell, including electron-hole direct, electron-Mn, and hole-Mn exchange interactions, a small anisotropy of the quantum dot, and the electron-hole exchange interaction [21]. There are six emission peaks associated with $M_Z = -5/2, \ldots, +5/2$. The predicted peak spacing $\Delta_{i(M_Z)}$ $i = 1$–5, plotted in Fig. 3(b) in light gray (green), decreases linearly with increasing i or M_Z. This decrease is reproduced by numerical calculations and experiment (black line). Deviations from linear dependence of Δ_{M_Z} are due to the electron-hole exchange interaction and anisotropy. The inset of Fig. 3(b) confirms the characteristic pattern of spacings between the X-Mn emission peaks for ten different quantum-dot samples.

Finally, Fig. 4 shows the calculated absorption spectra. We see the s shell, the two excited exciton states associated with $|PP\rangle$ and $|SD\rangle$ configurations in the energy range of the p shell, and the d shell. The shells are split into a fine structure by the presence of Mn. Different colors of the

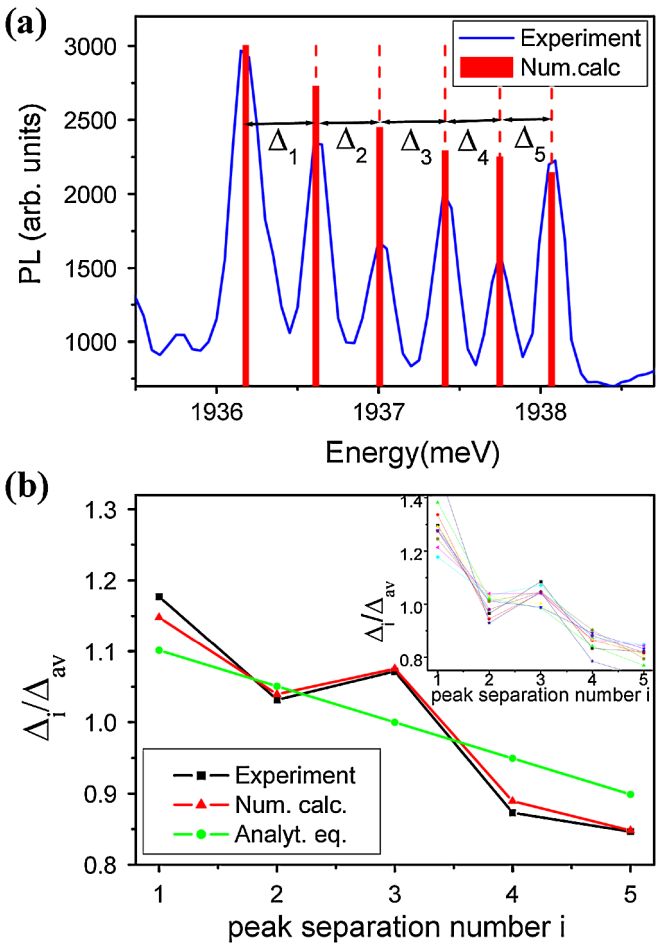

FIG. 3 (color online). (a) Measured and calculated s-shell emission spectrum at temperature $T = 75$ K including small anisotropy ($\gamma_{e(h)} = 0.33$ corresponding to $\omega_y/\omega_x = 0.71$) and electron-hole exchange interaction $\Delta_0 = 0.5$ meV, $\Delta_2 = 0.16$ meV, for the quantum dot with single-particle energies $\omega_e + \omega_h = 30$ meV; $\omega_e/\omega_h = 4$. (b) Comparison of the measured and calculated peak separation $\Delta_{i(M_Z)}/\Delta_{\mathrm{av}}$ (Δ_{av} being the average distance) as a function of the peak separation number i. The inset shows measured $\Delta_i/\Delta_{\mathrm{av}}$ for ten quantum dots from the same wafer. The green line shows $\Delta_{i(M_Z)}/\Delta_{\mathrm{av}}$ calculated analytically (neglects anisotropy and electron-hole exchange interaction).

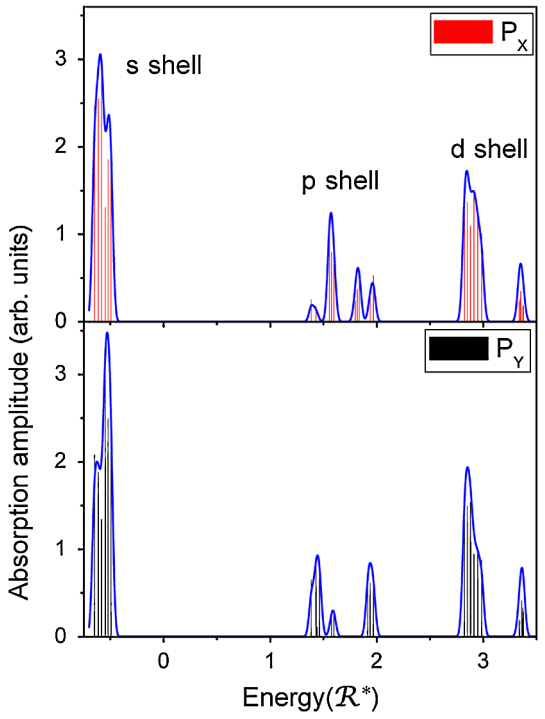

FIG. 4 (color online). Absorption spectrum calculated for a CdTe quantum dot with parameters as in Fig. 3 (top, P_x; bottom, P_y polarization).

peaks correspond to the degree of linear polarization of absorbed photons, with black (red) denoting the p_y (p_x) polarization. In this spectrum we identify the two consequences of the existence of the d shell: the complex emission pattern in the p-shell range of energies and the QI in the s shell. The p-shell electron-hole exchange splitting is larger than the s and d shell, leading to a much stronger linear polarization of the emission lines. Experiments are on the way to verify the predicted absorption spectra.

In summary, we formulated a microscopic description of the exciton-Mn interaction which includes correlations in the electron–valence-hole complex, the short-range exchange of Mn ion with the hole and the electron, the long-range electron-hole exchange, and the quantum-dot anisotropy. A new QI effect between the electron-hole Coulomb scattering and the scattering by Mn ion has been predicted and observed in the emission spectra as the decrease of emission peak spacing with increasing state of the Mn ion. This opens the possibility of engineering exciton-Mn spin interaction in quantum dots via quantum interference for quantum memory and information processing applications.

The authors thank NRC-CNRS CRP, NSERC, Canadian Institute for Advanced Research, QuantumWorks, and Polish Ministry of Science and Higher Education for support.

[1] A. J. Heinrich *et al.*, Science **306**, 466 (2004).
[2] S. Loth *et al.*, Nature Phys. **6**, 340 (2010).
[3] S. C. Erwin *et al.*, Nature (London) **436**, 91 (2005).
[4] S. T. Ochsenbein *et al.*, Nature Nanotech. **4**, 681 (2009).
[5] D. A. Bussian *et al.*, Nature Mater. **8**, 35 (2008).
[6] A. Hundt, J. Puls, and F. Henneberger, Phys. Rev. B **69**, 121309(R) (2004).
[7] L. Besombes *et al.*, Phys. Rev. Lett. **93**, 207403 (2004).
[8] C. Le Gall *et al.*, Phys. Rev. B **81**, 245315 (2010).
[9] M. Goryca *et al.*, Phys. Rev. Lett. **103**, 087401 (2009).
[10] A. Kudelski *et al.*, Phys. Rev. Lett. **99**, 247209 (2007).
[11] J. Fernandez-Rossier, Phys. Rev. B **73**, 045301 (2006).
[12] S.-J. Cheng and P. Hawrylak, Europhys. Lett. **81**, 37 005 (2008).
[13] A. O. Govorov and A. V. Kalameitsev, Phys. Rev. B **71**, 035338 (2005).
[14] D. E. Reiter, T. Kuhn, and V. M. Axt, Phys. Rev. Lett. **102**, 177403 (2009).
[15] A. Richardella *et al.*, Science **327**, 665 (2010).
[16] D. Goldhaber-Gordon *et al.*, Nature (London) **391**, 156 (1998).
[17] M. Bayer *et al.*, Nature (London) **405**, 923 (2000).
[18] P. Hawrylak *et al.*, Phys. Rev. Lett. **85**, 389 (2000).
[19] S. Raymond *et al.*, Phys. Rev. Lett. **92**, 187402 (2004).
[20] P. Hawrylak, Phys. Rev. Lett. **71**, 3347 (1993).
[21] E. S. Kadantsev and P. Hawrylak, Phys. Rev. B **81**, 045311 (2010).
[22] A. H. Trojnar *et al.* (to be published).
[23] F. Qu and P. Hawrylak, Phys. Rev. Lett. **95**, 217206 (2005).
[24] W. Sheng and P. Hawrylak, Phys. Rev. B **73**, 125331 (2006).
[25] P. Wojnar *et al.*, Phys. Rev. B **75**, 155301 (2007).
[26] Y. Leger *et al.*, Phys. Rev. Lett. **95**, 047403 (2005).